

Study on Properties of thin Tungsten Coatings Prepared in Na₂WO₄ Molten Salt

Wenxuan Qin^{1,2}, Xiaoli Xi^{1,2,*}, Qinghua Zhang¹, Liwen Zhang¹, Liwen Ma², Zuoren Nie^{1,2}

¹ National Engineering Laboratory for Industrial Big-data Application Technology, Beijing University of Technology, Beijing 100124, China

² College of Materials Science and Engineering, Key Laboratory of Advanced Functional Materials, Education Ministry of China, Beijing University of Technology, Beijing 100124, China

*E-mail: qinwenxuan123@emails.bjut.edu.cn; xixiaoli@bjut.edu.cn ;

Received: 28 June 2019 / Accepted: 7 August 2019 / Published: 7 October 2019

In this paper, tungsten coatings on copper substrates were prepared by electro-deposition from a Na₂WO₄ molten salt system at 1173K. The coating composition, microstructure, and morphology were studied via XRD, SEM, EDS, and LSCM. The electrochemical reduction mechanism of W⁶⁺ in the Na₂WO₄ system was investigated by cyclic voltammetry and square wave voltammetry. The results demonstrate that the tungsten coatings obtained under different process parameters are free from impurities. At a current density of 20 mA/cm², the tungsten coating shows no apparent crystal plane orientation, and a dense tungsten coating with a preferred orientation along the (211) plane is obtained as the current density increases. As the electrodeposition duration increases, the (211) crystal plane texture coefficient increases. The tungsten reduction process in the molten salt system at 1173 K follows a two-steps reaction, W(VI)→W(IV)→W.

Keywords: Molten salt; Electrodeposition; Tungsten coatings; Electrochemical Mechanism

1. INTRODUCTION

Tungsten is one of the most important rare refractory metals that shows excellent properties, such as a high melting point, a high temperature strength, a high hardness, a low electron work function, and a good chemical stability. Due to its unique properties, it is deemed as a promising material in electronic industries, fusion devices, and aerospace applications [1-4]. However, bulk tungsten has the disadvantage of being hard and brittle, and this generates difficulties during its formation and processing [5]. As an alternative, coating technologies are used to combine tungsten with heat sink materials in several applications. In addition, tungsten materials are relatively expensive when compared to conventional heat sink materials such as copper. Copper-based heat sink materials have an excellent

thermal conductivity and process-ability. Thus, the W coating is a valuable composite material that can be coated on copper substrates [6, 7].

Currently vacuum plasma spraying (VPS) [8], physical vapor deposition (PVD) [9], and chemical vapor deposition (CVD) [10] techniques are widely used in the preparation of tungsten coatings. However, these methods still have some disadvantages, such as the introduction of impurity phases, the high oxygen content of the coatings, environmental pollution, and high cost, [11]. Researchers are constantly investigating less expensive and simpler technologies to obtain better coatings. The electrodeposition technology is a very effective method. However, tungsten is a metal that cannot be separated from a brine solution, due to the co-deposition of metals from the Fe, Ni, Co ferrous groups. Thus, the pure and dense tungsten coatings must be electrodeposited from a molten salt system. [12-15]. Nowadays, the technology of electrodeposited metallic tungsten coatings from a molten salt is relatively mature. As a result, researchers have separately deposited tungsten coatings from different molten salt systems. For instance, they were electrodeposited from in Zinc bromide-sodium bromide and zinc chloride-sodium chloride molten salt systems at 623–723 K [16, 17]. Nakajima et al. electrodeposited tungsten from molten $\text{ZnCl}_2\text{-NaCl-KCl-WCl}_4$ and $\text{ZnCl}_2\text{-NaCl-KCl-KF-WO}_3$ at 523 K [18, 19]. Domestic scientists have also done a lot of work on molten salt electrodeposited tungsten. Ma et al [20]. prepared tungsten coatings in $\text{Na}_2\text{WO}_4\text{-ZnO-WO}_3$ by applying a pulse current. Zhang and Jiang et al [21-24]. conducted several studies on the electrodeposited tungsten coatings from a $\text{Na}_2\text{WO}_4\text{-WO}_3$ binary system.

Generally speaking, the molten salt system of electrodeposited tungsten is divided into solvent and solute, and the tungsten source generally exists as a solute. The electrodeposition of tungsten coatings in single element molten salt system has not been reported in the literature yet. In this work, tungsten coatings were electrodeposited in a single Na_2WO_4 molten salt system and tungsten coatings were prepared via electrodeposition on Cu substrates under various conditions in a Na_2WO_4 system. The effects of the current density and electrodeposition duration on the composition, structure, and properties of the tungsten coatings were investigated experimentally. The electrochemical reaction process of the tungsten ions in the molten salt systems was also investigated.

2. EXPERIMENT

The chemical reagents used are analytically pure, and they were dried in a furnace at 443 K for 24 hours. The dried chemicals were placed in an alumina crucible and then, direct current electrodeposition was carried out in a vacuum tube furnace at 1173 K using an electrochemical workstation (P4000). The schematic diagram of the device is shown in Fig. 1. A three-electrode system was used during the experiment, the working electrode consisted of a Cu substrate (10 mm × 6 mm × 1 mm), whereas the counter electrode was a tungsten rod (Φ 3.2 mm × 25 mm), Moreover, a Pt wire (Φ 0.5 mm × 25 mm) was used as the reference electrode. The electrode surfaces were polished prior to electrodeposition to remove possible scratches of the surface, voids, and stains. The samples were then cleaned in an acetone and distilled water in an ultrasonic bath in this order. The tungsten coatings were prepared on copper substrates with current densities of 20, 40, 60, 80 mA/cm² using DC deposition for

6 hours. In addition, at a current density of 40 mA/cm^2 , a direct current electrodeposition was used for 6h, 7h, 8h, and 9h. After electrodeposition, the obtained coatings were immediately immersed in an aqueous NaOH solution (5 mol/L) to remove the adhered salts and then, ultrasonically washed in distilled water.

The microstructure, morphologies and roughness of the coatings were examined via scanning electron microscopy (SEM, SEM-2100) and laser confocal microscopy (LSCM, LSCM-OLS4100). Furthermore, the phase composition and crystal orientation of the deposit were measured via X-ray diffraction (XRD, XRD-6000). All the electrochemical performance tests were carried out by using a P4000 electrochemical workstation equipped with the Versa Studio software package (Advanced Measurement Technology, Inc., USA). All the electrochemical process tests were performed in a high purity Ar gas atmosphere. The electrochemical experiments require the use of a three-electrode system, where the counter electrode consists of a graphite rod ($\Phi 2 \text{ mm} \times 20 \text{ mm}$), whereas both the working and the reference electrodes are platinum wires ($\Phi 0.5 \text{ mm} \times 25 \text{ mm}$). The electrodes are polished and their extremities, which are inserted into the molten salt portion, must be smooth and flat. Finally, all the electrodes were ultrasonically cleaned with alcohol and dried. The electrochemical techniques used in this work include cyclic voltammetry and square wave voltammetry to study the electrochemical reaction of W ions on the electrodes at 1173 K. Cyclic voltammetry was used at different scan rates in a 0.075 - 0.175 V/s range.

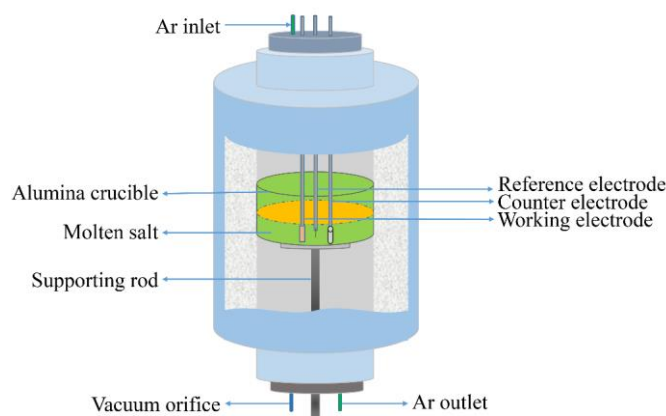


Figure 1. Schematic diagram of the device

3. RESULTS AND DISCUSSION

3.1 Preparation of tungsten coatings for different electrodeposition durations

3.1.1 Composition and microstructure

Fig. 2 (a) shows the XRD pattern of the coatings obtained for different electrodeposition durations: the coatings consist of pure tungsten and no impurity phase was detected. The results also show that the tungsten obtained is α -W, which is a body-centered cubic structure.

In order to describe in detail the preferred orientation of the coatings, the texture coefficient ($TC_{(hkl)}$) can be calculated by using the following formula (1):

$$TC_{(hkl)} = \frac{I'_{(hkl)}/I_{(hkl)}}{1/N[\sum I'_{(hkl)}/I_{(hkl)}]} \quad (1)$$

Where $TC_{(hkl)}$ is the texture coefficient of the crystal plane, $I'_{(hkl)}$ is the actual diffraction intensity along the (hkl) crystal plane, $I_{(hkl)}$ is the standard diffraction intensity along the tungsten (hkl) crystal plane, and N is the number of growth orientations [25].

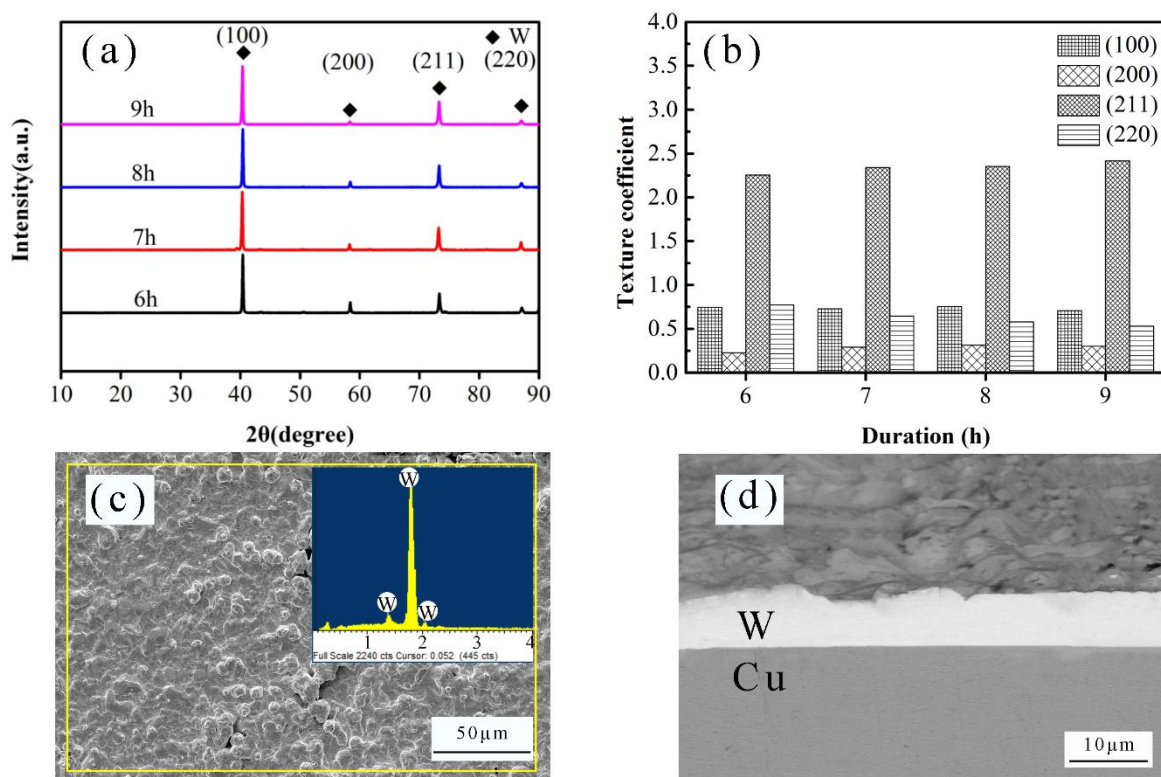


Figure 2. (a) XRD patterns of tungsten coatings obtained for different electrodeposition durations; (b) Texture coefficient of tungsten coatings obtained at different electrodeposition durations; (c) Surface SEM image and EDS analysis of the tungsten coating obtained after 8 h; (d) Cross-sectional SEM image of the tungsten coating obtained after 8 h.

The texture coefficients of the tungsten coatings obtained for different electrodeposition durations are presented in Fig. 2 (b). The results show that after electrodeposition for different durations the (211) planes of the metal tungsten coatings exhibit a distinct preferred orientation. Moreover, as the electrodeposition duration increases, the (211) crystal plane texture coefficient increases continuously.

The analysis of the surface SEM-EDS and the cross-sectional morphology of the tungsten coating obtained after 8 h are shown in Fig. 2 (c) and Fig. 2 (d). The coating consists of pure metal tungsten with no cracks or holes (Fig. 2 (c)). Fig. 2 (d) shows that a thin tungsten coating with a uniform thickness is obtained by electrodeposition after 8 h and that the average thickness of the coating measures about 6.97 μm.

3.1.2 Surface morphologies and properties of the tungsten coatings

The roughness of the tungsten coatings was analyzed via laser confocal microscopy. Figure 3 includes the morphology and linear skeleton diagrams of the coatings surface for different electrodeposition durations. The results show that the surface roughness of the coatings increases as the electrodeposition duration increases. In this paper, the Ra value is used to indicate the surface roughness of the coating. When the electrodeposition duration is 6 h, the surface roughness of the tungsten coating measures 0.956 μm . Upon the increase of the electrodeposition duration, the surface roughness increases continuously. When the electrodeposition duration is 9 h, it reaches its maximum of 4.308 μm .

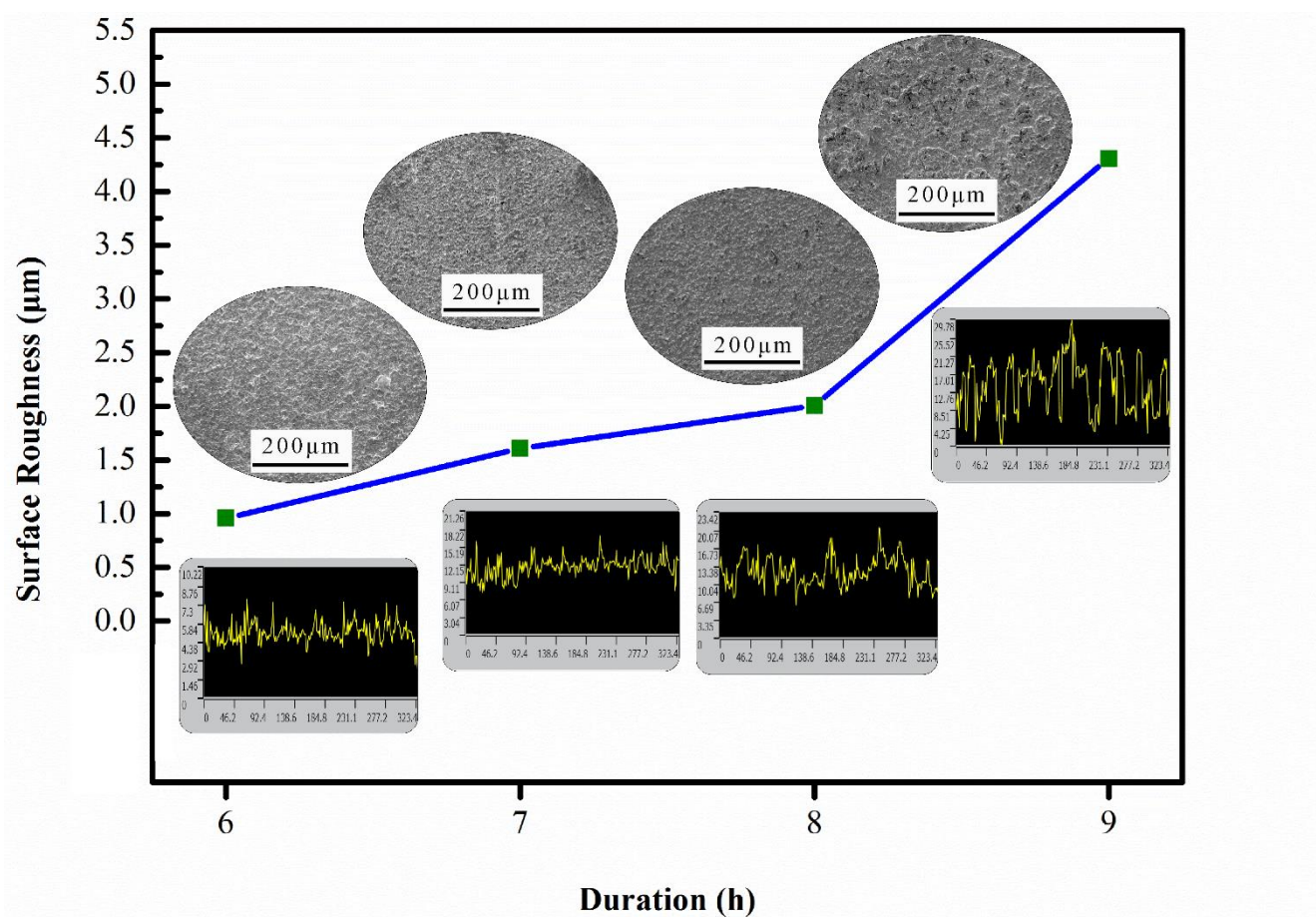


Figure 3. Surface morphologies, profiles, and roughness of the electrodeposition tungsten coatings obtained for different electrodeposition durations.

It can also be seen from Fig. 3 that dense tungsten coatings with no obvious cracks and holes can be obtained for different electrodeposition durations. However, these coatings still show obvious differences in their morphology. When the electrodeposition duration is 6 h, the surface of the coating is smooth and uniform. Upon the increase in the electrodeposition duration up to 8 h, nodules are

observed on the coating surface. As the duration of the reaction increases further, the nodules continue to grow and the surface quality decreases.

The formation of the tungsten coatings is related to the electrochemical crystallization process [26]. As the electrodeposition duration increases, the growth rate of the tungsten grains is higher than that for tungsten nucleation, and the grains grow continuously. When the electrodeposition process progresses, tungsten ions near the cathode are continuously consumed since the absorption rate of the tungsten ions near the cathode is higher than their replenishment rate, a concentration polarization generated and the dispersing ability of the molten salt decreases. Then growth rate of the coarse grains produced on the surface of the coatings accelerates, whereas the growth of small grains decreases, inducing an increase in the roughness. As the electrodeposition duration further increases, the grains aggregate to form nodules.

3.2 Preparation of tungsten coatings for different current densities

3.2.1 Composition and microstructure

The XRD patterns of the coatings obtained when different current densities are applied are shown in Figure 4 (a). Unmixed tungsten coatings can be obtained at different current densities and the tungsten crystal structure belongs to the body-centered cubic structure.

The texture coefficient $TC(h\ k\ l)$ of the tungsten coating for different current densities can be calculated via Formula (1). Moreover, the texture orientations are used to determine the preferred orientation of the coating.

Fig. 4 (b) shows the texture coefficients of the tungsten coatings for different current densities. There is no apparent crystal plane orientation when the current density measures 20 mA/cm^2 and tungsten coatings with stronger preferred orientation along the (211) plane can be obtained at higher current densities. As the current density changes from 40 mA/cm^2 to 80 mA/cm^2 , the results show that the coatings are all highly (211)-orientated.

The SEM micrographs together with the EDS analysis of the tungsten coating obtained at 60 mA/cm^2 are shown in Fig. 4 (c). The results confirm that the coating is composed of tungsten. Fig. 4 (d) shows the cross-sectional SEM micrograph of the tungsten coating obtained at 60 mA/cm^2 : the bond between the coating and the copper substrate is excellent, there are no cracks or holes, and the coating thickness is uniform (about $7.64\ \mu\text{m}$).

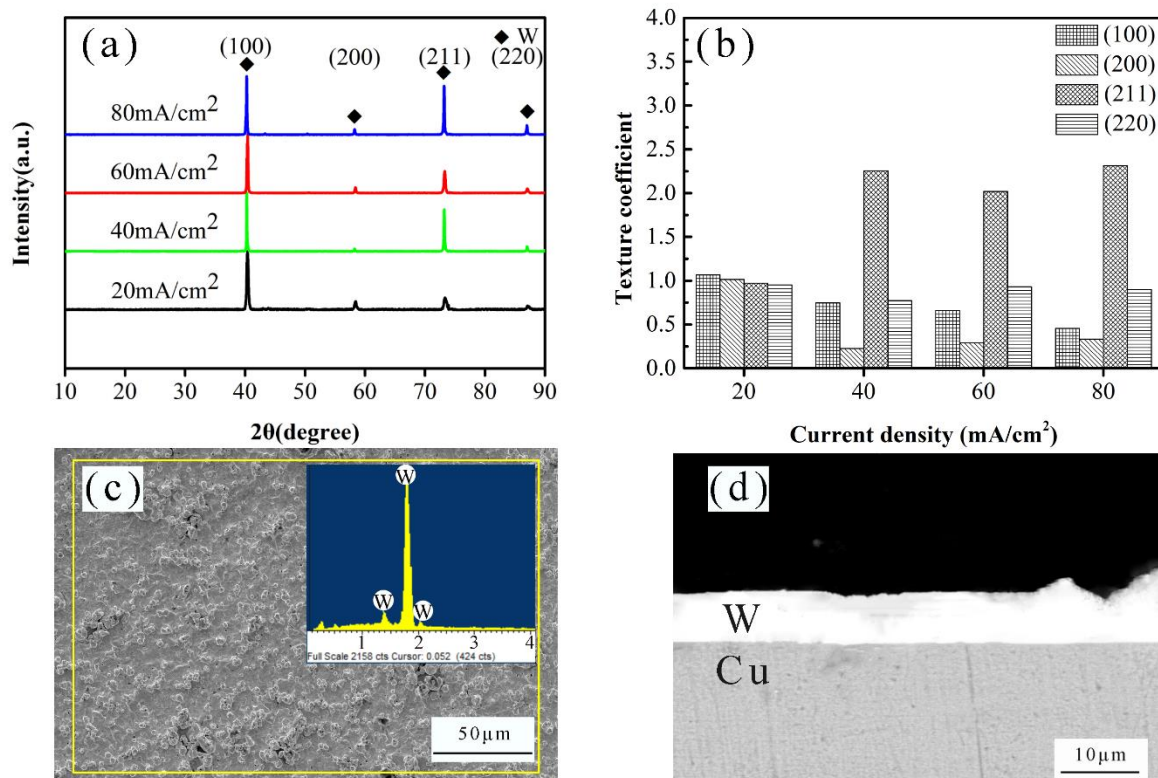


Figure 4. (a) XRD patterns of the tungsten coatings obtained for different current densities; (b) Texture coefficient of the tungsten coatings obtained for different current densities; (c) Surface SEM image together with the EDS analysis of the tungsten coating obtained at 60 mA/cm²; (d) Cross-sectional SEM image of the tungsten coating obtained at 60 mA/cm².

3.2.2 Surface morphologies and properties of the tungsten coatings

Figure 5 is a graph showing the surface topographies, the linear profiles, and the surface roughness of the tungsten coatings obtained at different current densities. The coating exhibits obvious pores at a current density of 20 mA/cm² and dense tungsten coatings can be obtained at current densities higher than 40 mA/cm². However, as the current density increases, significant differences appear in the surface morphology and roughness of the coatings. When the current density reaches 60 mA/cm², obvious coarse grains are present on the surface of the coating and its flatness is reduced. Figure 5 also shows that the surface roughness of the coating increases as the current density increases. When the current density reaches 20 mA/cm², the surface roughness of the tungsten coating measures 0.706 μm. As the current density increases, the surface roughness of the coating increases continuously. When the current density is 80 mA/cm², the surface roughness of the coating reaches its maximum (4.006 μm).

As the dispersion of the electrolyte decreases, the growth rate of the coarse grains exceeds the other fine grains on the electrodeposited surface. Thus, the preferential growth of these grains results in an increase in the number of nodules and in the surface roughness.

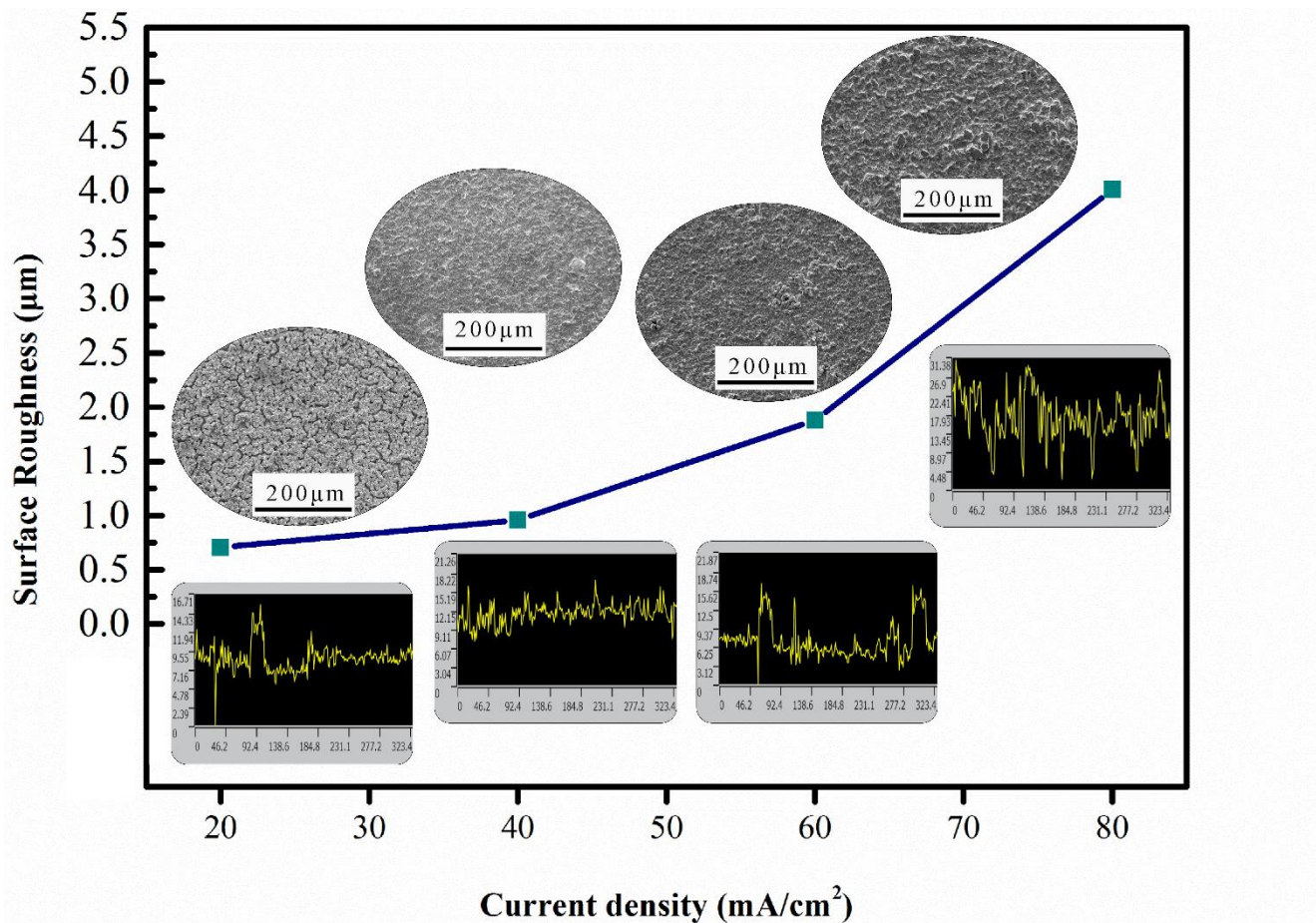


Figure 5. Surface morphologies, profiles and roughness of the electrodeposition tungsten coatings obtained for different current densities.

3.3 Electrochemical reaction process

Figure 6 (a) shows the cyclic voltammetry curve obtained at different scan rates in the Na₂WO₄ molten salt system at 1173 K. The scan rate ranges is 0.075–0.175 V/s and two pairs of redox peaks appear in the cyclic voltammetry curve. As the scan rate increases, no significant change in the position of the current peaks is detected. Moreover, the peak current increases with the scan rate. Square wave voltammetry is generally used to quantitatively investigate the number of transferred electrons of tungsten ions reduction during the electrolysis, due to its high sensitivity. The square wave voltammetry curve is shown in Fig. 6 (b). The results show that two cathode reduction peaks are present in the curve. The two reduction peaks correspond to the two reduction peaks observed in the cyclic voltammetry curve. The Gaussian fit of the data of the square wave voltammetry curve provides the measurement of the half width of the peak of the tungsten ions cathode reduction reaction. Using Formula (2), the number of electrons transferred from the tungsten ions during the electrode reaction can be calculated as follows [27]:

$$W_{1/2} = 3.52 \times \frac{RT}{nF} \tag{2}$$

Here, $W_{1/2}$ corresponds to the half width of the reduction peak, R is the gas constant, T is the experimental temperature (K), n is the number of transferred electrons, and F is the Faraday constant (96485 C/mol).

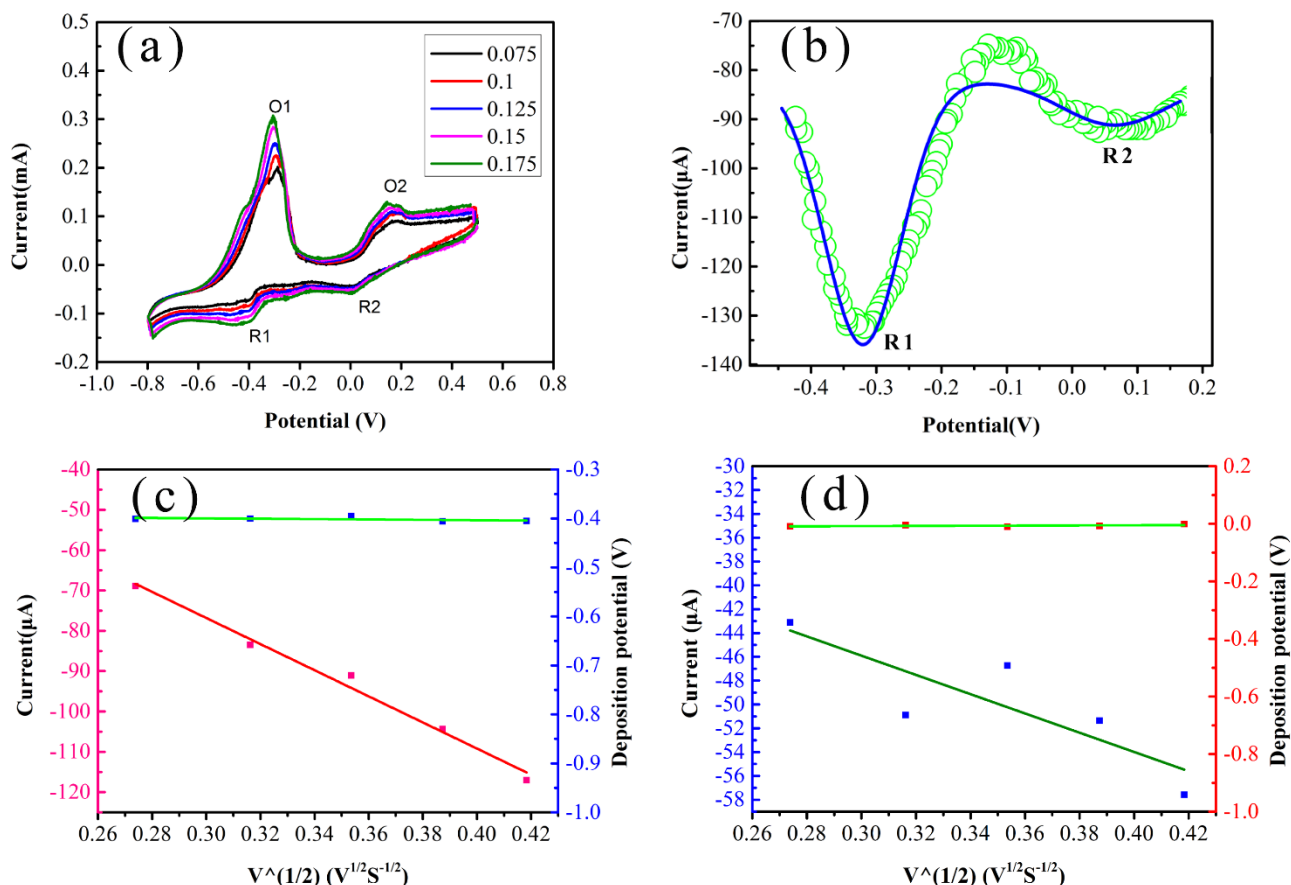


Figure 6. (a) Cyclic voltammety curve obtained at different scan rates in the Na_2WO_4 molten salt system at 1173 K; (b) Square wave voltammety curve of the 1173 K Na_2WO_4 molten salt system; (c) Relation between the R1 peak deposition potential, the deposition peak current, and the square root of the scan rate (d) Relation between the R2 peak deposition potential, the deposition peak current, and the square root of the scan rate.

By calculating the half width value of the reduction peak (Fig. 6 (b)), one can conclude that the electron transfer number of the reduction peak R1 is equal to about 4, whereas the electron transfer number of the reduction peak R2 is 2. Therefore, the W(VI) of the tungstate ions reduction process is completed in two steps and the reduction reaction is $\text{W(VI)} \rightarrow \text{W(IV)} \rightarrow \text{W}$. Moreover, Liao et al [28]. showed that the reduction of the tungsten ions undergoes a two-steps reaction. In addition, Brett et al [29]. inferred that the transformation reaction of WO_3 into the W metal is likely to be $\text{WO}_3 \rightarrow \text{WO}_2 \rightarrow \text{W}$. These conclusions are consistent with the results of this study.

Figures 6 (c) and 6 (d) show that, as the scan rate increases, the reduction potential of the tungsten ions remains constant at -0.4V and 0V. The reduction peak current of the tungsten ions shows a linear trend as a function of the square root of the scan rate and the curve passes through the origin. These

results indicate that the two-steps reaction of the tungsten ions is a reversible reaction controlled by diffusion [30].

4. CONCLUSION

In this paper, pure tungsten coatings were obtained by varying the experimental parameters in a single Na_2WO_4 molten salt system. Moreover, the effects of the current density and of the electrodeposition duration on the structure and properties of the coatings were explored. In addition, the electrochemical reaction mechanism of tungsten was determined via a series of electrochemical testing techniques. The results show that the cathode current density and the electrodeposition time have an important influence on the structure and the surface properties of the tungsten coatings. As the current density increases, the metal tungsten exhibits a preferred orientation along the (211) plane. Furthermore, the coating crystal grains become gradually denser and the roughness increases continuously. Upon the increase in the electrodeposition duration, the preferred orientation of the (211) plane becomes more and more obvious, the coatings roughness increases continuously, and nodules appear on the coating surfaces. The reduction process of tungsten in molten salt system at 1173 K is a two-steps reaction, which follows the mechanism: $\text{W(VI)} \rightarrow \text{W(IV)} \rightarrow \text{W}$.

ACKNOWLEDGEMENTS

This work was supported by National Natural Science Foundation of China (51621003), Beijing Municipal Natural Science Foundation (2172010) and the Fundamental Research Funds for Science and Technology Innovation Service Capacity-building (Beijing municipal level PXM2019_014204_500032).

References

1. A. Terra, G. Sergienko, M. Tokar, D. Borodin, T. Dittmar, A. Huber, A. Kreter, Y. Martynova, S. Möller, M. Rasiński, M. Wirtz, T. Loewenhoff, D.D. Gerspach, Y. Yuan, S. Brezinseka, B. Unterberga and C. Linsmeier, *Nucl. Mater. Energy*, 19 (2019) 7.
2. J. Webb, S. Gollapudi and I. Charit, *Int. J. Refract. Met. Hard Mater.*, 82 (2019) 69.
3. A. Kobayashi, S. Sharafat and N.M. Ghoniem, *Surf. Coat. Tech.*, 200 (2006) 4630.
4. H.Y. Wu, Y. Li, Y.Z. Wang, Z. Ping and W.F. Rao, *J. Rare Earths*, 34 (2016) 958.
5. Y.F. Qi, Y.H. Tang, B. Wang, M. Zhang, X.Q. Ren, Y.G. Li and Y.T. Ma, *Int. J. Refract. Met. Hard Mater.*, 81 (2019) 183.
6. F. Jiang, Y.C. Zhang, X.Y. Yang and K. Huang, *Mater. Res. Express*, 6 (2019) 16502.
7. A. Gusarov, C. Pohl, T. Pfalz, R.W. Bosch, S.V. Dyck, V. Barabashc, R. Eatonc, F. Zacchiad and H. Samuli, *Fusion Eng. Des.*, 137 (2018) 112.
8. H.S. Kim, B.G. Hong and S.Y. Moon, *Thin Solid Films*, 623 (2017) 59.
9. H. Kim, H.J. Lee, S.H. Kim and C. Jang, *Fusion Eng. Des.*, 111 (2016) 590.
10. J.Q. Shi, Y.B. Shen, S.Y. Yao, P.J. Zhang, Q. Zhou, Y.Z. Guo, C.W. Tan, X.D. Yu, Z.H. Nie, H.L. Ma and H.N. Cai, *Mater. Charact.*, 122 (2016) 36.
11. N.B. Sun, Y.C. Zhang, F. Jiang, S.T. Lang and M. Xia, *Fusion Eng. Des.*, 89 (2014) 2529.
12. A. Bodaghi and J. Hosseini, *Int. J. Electrochem. Sci.*, 7 (2012) 2584.
13. M. Jaksender, E. Miękoś, M. Zieliński, K. Kołodziejczyk, D. Sroczynski, A. Łukawska, D.

- Szczukocki, B. Krawczyk, K. Czarny and R. Juszcak, *Int. J. Electrochem. Sci.*, 13 (2018) 6897.
14. Y.H. Liu, Y.C. Zhang, Q.Z. Liu, X.L. Li, F. Jiang and C.C. Ge, *Electroplat. Finish.*, 31 (2012) 1004.
 15. R.X. Ma, C.H. Zhou, G.X. Li, C.Q. Wang and L.H. Sun, *Chin. J. Nonferrous Met.*, 10 (2000) 715.
 16. A. Katagiri, M. Suzuki and Z. Takehara, *J. Electrochem. Soc.*, 138 (1991) 767.
 17. M. Masuda, H. Takenishi and A. Katagiri, *J. Electrochem. Soc.*, 148 (2001) C59.
 18. H. Nakajima, T. Nohira and R. Hagiwara, *Electrochem. Solid-State Lett.*, 8 (2005) C91.
 19. H. Nakajima, T. Nohira, R. Hagiwara, K. Nitta and S. Inazawa, *Electrochim. Acta*, 53 (2007) 24.
 20. R.X. Ma, W. Ling, Z.L. Wu and B. Kang and M.K. Wang, *Mater. Sci. Technol.*, 17 (2009) 754.
 21. F. Jiang, *Appl. Surf. Sci.*, 363 (2016) 389.
 22. F. Jiang, Y.C. Zhang, N.B. Sun and J.X. Len, *Appl. Surf. Sci.*, 331 (2015) 278.
 23. F. Jiang, Y.C. Zhang, N.B. Sun and J.X. Len, *Appl. Surf. Sci.*, 327 (2015) 432.
 24. F. Jiang, Y.C. Zhang, X.L. Li, N.B. Sun and L.L. Wang, *Fusion Eng. Des.*, 89 (2014) 818.
 25. F. Jiang, Y.C. Zhang and X.L. Li, *Fusion Eng. Des.*, 93 (2015) 30.
 26. Y.H. Liu, Y.C. Zhang, Q.Z. Liu, X.L. Li and F. Jiang, *Fusion Eng. Des.*, 87 (2012) 1861.
 27. W. Wu, S.Q. Guo and J.S. Zhang, *Int. J. Electrochem. Sci.*, 13 (2018) 225.
 28. C.F. Liao, M.Z. Fang, X. Wang, H. Tang and L.S. Luo, *Nonferrous Met. Sci. Eng.*, 6 (2015) 6.
 29. R. Abdulaziz, L.D. Brown, D. Inman, P.R. Shearing and D.J.L. Brett, *Electrochimica. Acta*, 226 (2017) 18.
 30. T.B. Joseph, N. Sanil, L. Shakila, K.S. Mohandas and K. Nagarajan, *Electrochimica. Acta*, 139 (2014) 394.

© 2019 The Authors. Published by ESG (www.electrochemsci.org). This article is an open access article distributed under the terms and conditions of the Creative Commons Attribution license (<http://creativecommons.org/licenses/by/4.0/>).